

## Magnetism of ordered Sm/Co(0001) surface structures

J.E. Prieto<sup>1</sup>, O. K. Rupin<sup>1</sup>, S. Gorovikov<sup>2</sup>, K. Dobrich<sup>1</sup>, G. Kaindl<sup>1</sup>, and K. Starke<sup>1</sup><sup>1</sup>Institut für Experimentalphysik, Freie Universität Berlin, Am Müllberg 14, D-14195 Berlin, Germany<sup>2</sup>MAX-Lab, Lund University, P.O. Box 118, Lund S-22100, Sweden

(dated: March 23, 2024)

The epitaxial system Sm/Co(0001) was studied for Sm coverages up to 1 monolayer (ML) on top of ultrathin Co/W (110) epitaxial films. Two ordered phases were found for 1/3 and 1 ML Sm, respectively. The valence state of Sm was determined by means of photoemission and magnetic properties were measured by magneto-optical Kerr effect. We find that 1 ML Sm causes a strong increase of the coercivity with respect to that of the underlying Co film. Element-specific hysteresis loops, measured by using resonant soft x-ray reflectivity, show the same magnetic behaviour for the two elements.

PACS numbers: 75.70.Ak, 78.20.Ls, 61.14.Hg, 61.10.-i, 79.60.-i

## I. INTRODUCTION

Magnetic metals can be classified into two main groups. On the one hand, the transition metals (TMs), where the magnetic moments are carried by the partly itinerant, strongly overlapping 3d electrons. Due to strong crystal-field splittings, the orbital moments are mostly quenched, and the magnetic moments have predominantly spin character. The magnetic coupling is therefore strong, giving rise to ordering temperatures as high as 1000 K, while the magnetic anisotropies are relatively small. On the other hand, rare-earth (RE) magnetism is determined by the localized, atomic-like character of the magnetic moments of the 4f shell, which in general contain both a spin and an orbital part. Non-vanishing orbital moments give rise to non-spherical 4f charge distributions that lead to strong "single-ion" contributions to the magnetic anisotropy. The very small overlap between the 4f orbitals of neighbouring atoms is responsible for a negligible direct exchange interaction between the 4f moments of RE ions. Instead, they couple indirectly through the conduction electrons (RKKY interaction), a mechanism that leads to ordering temperatures typically lower than room temperature (RT) in RE metals.

Some intermetallic compounds containing both RE and TM ions combine the magnetic properties of the two classes of components. For example, the Co-Sm and Nd-Fe-B systems include the magnetically hardest materials known today. In these compounds, the high magnetic anisotropies are induced by the RE ions, while the characteristic high ordering temperatures of the ferromagnetic TMs are retained<sup>1</sup>.

The trend in magnetic storage technology towards ever higher densities requires to reduce system dimensions to a degree where the superparamagnetic limit is approached<sup>2</sup>. A possible solution is the development of thin

films of materials with high magnetic anisotropy energies per unit volume that could retain high ordering temperatures and high coercivities at RT even when system sizes approach the nanometer scale. A promising material is Co<sub>5</sub>Sm, in which a relatively small fraction of the RE

metal Sm renders the material much harder than pure Co<sup>3,4</sup>. Hence, it is interesting to study the effect of Sm on the magnetic properties of very thin Co films.

Here, we report on a study of the epitaxial system Sm/Co(0001) on W (110) with Sm coverages up to 1 ML, where we found several ordered surface phases. Their magnetic properties were studied by means of visible-light and soft x-ray magneto-optical Kerr effect (MOKE), and their electronic structure was investigated by photoelectron spectroscopy.

## II. EXPERIMENTAL

Co films of about 10 ML thickness were prepared by metal vapour deposition in ultra-high vacuum (UHV) on a W (110) single-crystal substrate. To this end, a high-purity Co rod was heated by electron bombardment. Sm was deposited from a W crucible. The same substrate and evaporators were used in all experiments. Deposition rates were of the order of 1 ML per minute. The crystallinity of the surfaces was checked by low-energy electron diffraction (LEED) using a rear-view optics. MOKE hysteresis loops were recorded in situ employing a rotatable electromagnet with a soft-iron yoke<sup>5</sup>, with external magnetic fields up to 2 kOe applied in-plane along the substrate  $\text{bcc}[110]$  direction; this corresponds to the easy axis of magnetization of the thin epitaxial Co/W (110) films<sup>6</sup>. Resonant soft x-ray reflectivities using circularly-polarized (CP) light were measured for

films prepared in situ in the same UHV chamber attached to the UE52-SGM undulator beam line of BESSY II. The specularly reflected intensity was detected by a Si photodiode mounted on a home-made 2-goniometer inside the UHV chamber. PE experiments were performed on films prepared in the same way at the I-311 undulator beam line of MAX-Lab in Lund, Sweden, which is equipped with a display-type electron analyzer. Spectra shown here were measured at normal emission in the angle-integrated mode, with an acceptance angle of 12.5°.

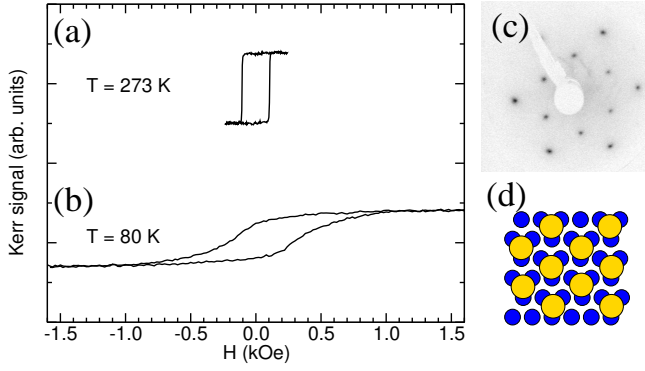


FIG. 1: Visible-light MOKE hysteresis curves of Sm (1/3 ML)/Co(8 ML)/(0001) measured at (a) 273 K and (b) 80 K. The LEED pattern for an electron energy of 150 eV, shown in (c) with inverted contrast, corresponds to a  $\begin{pmatrix} 1/3 & 1/3 \end{pmatrix}$ R30 superstructure. In (d), the proposed atomic structure of this phase (top view) is shown schematically; large and small circles represent Sm and Co atoms, respectively.

### III. RESULTS AND DISCUSSION

Epitaxial Co films on W (110) with thicknesses larger than about 5 ML show a  $\begin{pmatrix} 1 & 1 \end{pmatrix}$  LEED pattern of hexagonal symmetry (see, e.g. Fig. 2d), which reflects the fact that the hexagonal base planes of Co (0001) are parallel to W (110). In agreement with previous findings<sup>6,7,8,9</sup>, the growth proceeds in the Nishiyama-Wasserman orientation, i.e., the close-packed Co rows along  $[1\bar{1}20]$  run parallel to W  $[001]$ . In this thickness range, the epitaxial strain amounts to a few percent<sup>6</sup>. Upon deposition of 1/3 ML Sm, a  $\begin{pmatrix} 1/3 & 1/3 \end{pmatrix}$ R30 superstructure appears in the LEED pattern, as shown in Fig. 1c. The magnetization curves measured by visible-light MOKE on this surface are also shown in Fig. 1. At 273 K, the hysteresis loop has a square shape and the coercivity amounts to 100 Oe. Upon cooling down to 80 K, the coercivity increases to 250 Oe and the shape of the hysteresis becomes more elongated.

For higher Sm coverages, between 2/3 ML and 1 ML, a different LEED pattern appears. It is shown in Fig. 2c, in comparison with the hexagonal pattern of the clean Co film (Fig. 2d). The superstructure spots in Fig. 2c appear close to those of the  $\begin{pmatrix} 1/3 & 1/3 \end{pmatrix}$ R30 structure observed for lower coverages, but they now have an elongated shape along the tangential direction. The hysteresis curve measured for this phase at 80 K is shown in Fig. 2a. Compared with that of the clean Co film, the coercivity has increased from 230 to 630 Oe, i.e. by a factor of about 3. This effect allows to consider the Sm/Co/W (110) system as a prototype of a TM film with increased anisotropy due to the deposition of a small amount of a RE metal.

In Sm compounds, the electronic structure is strongly influenced by the valence state of the Sm ion. This is of particular importance for surface phases, because pure

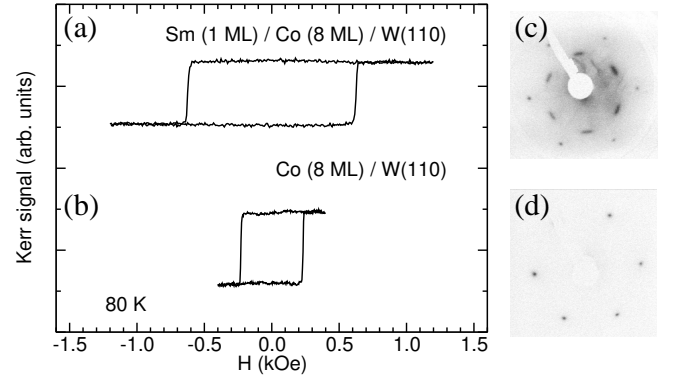


FIG. 2: (a) Visible-light MOKE hysteresis curve of Sm (1 ML)/Co(8 ML)/W (110) measured at 80 K. In (b), the corresponding curve measured under the same conditions for the 8 ML Co/W (110) in prior to Sm deposition is shown. LEED patterns (150 eV, inverted contrast) of the two surfaces are displayed in (c) and (d), respectively.

Sm metal is known to be trivalent in the bulk but divalent at the surface layer<sup>10</sup>. The reason is that the energy cost of promoting an electron from the 4f shell to the (6s5d) valence band is not compensated at the low-coordinated surface layer by stronger bonding. In order to determine the valence state of Sm, we performed PE experiments on both epitaxial Sm/Co(0001) phases using a photon energy of 141 eV to resonantly enhance the Sm features (4d-4f resonance). Figure 3 shows the valence-band PE spectra including the Sm 4f-multiplet structure. Both phases show strong emission in the region extending from the Fermi level to approximately 2 eV binding energy. This is caused by the partially filled 3d-band of Co. Furthermore, the characteristic set of peaks in the binding-energy region from 5 to 10 eV correspond to the final-state 4f multiplet reached from trivalent (4f<sup>5</sup>) Sm<sup>10</sup>.

The PE spectrum of the  $\begin{pmatrix} 1/3 & 1/3 \end{pmatrix}$ R30 phase contains only features characteristic for trivalent Sm<sup>10,11</sup>, i.e., Sm PE peaks at binding energies of 5.9, 8.3 and 10.0 eV. On the other hand, the 4f multiplet structure found for higher Sm coverages is shifted by 0.6 eV towards the Fermi level, so that the PE peaks appear at 5.3, 7.7 and 9.4 eV. In addition, the spectrum of Fig. 3b shows three features closer to the Fermi level, at binding energies of 0.8, 1.6 and 3.9 eV, respectively, which can be assigned to divalent (4f<sup>6</sup>) Sm ions<sup>11,12</sup>.

We interpret the  $\begin{pmatrix} 1/3 & 1/3 \end{pmatrix}$ R30 superstructure in terms of the formation of a magnetic Sm/Co surface phase. Based on the symmetry of the diffraction pattern as well as the known amount of deposited Sm (1/3 ML), we propose the model for the atomic arrangement in this phase that is shown in Fig. 1d; the Sm atoms occupy 3-fold coordinated sites on the topmost Co layer. From our analysis we cannot conclude which of the two inequivalent adsorption sites on the hexagonal close-packed sur-

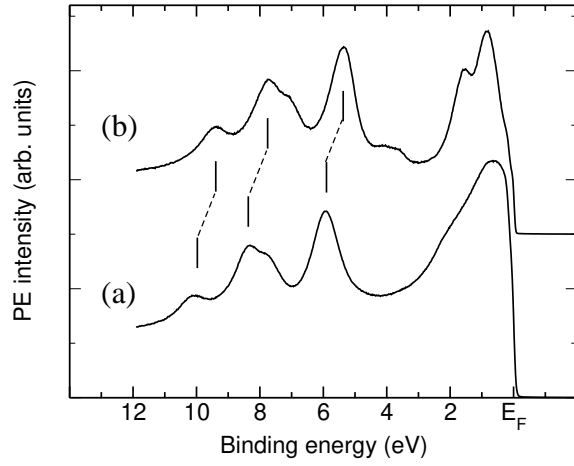


FIG. 3: Normal emission photoemission spectra of (a) Sm(1/3 ML)/Co/W(110) (showing the  $(\sqrt{3} \times \sqrt{3})R30$  superstructure) and (b) Sm(1 ML)/Co/W(110), both recorded with 141-eV photons. The shifts of the  $4f^5$  multiplet lines are indicated by vertical bars.

face layer (fcc or hcp) is preferred. The PE spectra in Fig. 3a show that the Sm ions are trivalent in this phase. The LEED pattern in Fig. 2c indicates for the Sm(1 ML) phase a similar structure as for the Sm(1/3 ML) phase showing the  $(\sqrt{3} \times \sqrt{3})R30$  superstructure, yet with some degree of rotational disorder. The 1-ML phase contains both trivalent and divalent Sm ions, as shown by the PE spectrum of Fig. 3b. This points towards the presence of "interface" and "surface" Sm atoms, assuming that further deposition of Sm on top of the  $(\sqrt{3} \times \sqrt{3})R30$  surface does not significantly distort the proposed structure.

The magnetic hysteresis curves of Sm(1/3 ML)/Co/W(110) at 80 K (Fig. 1b) show a more complex shape than that of the Sm(1 ML) phase at the same temperature (Fig. 2a). Besides lower coercivity, it reveals a reduced remanence. This may be due to a partial reorientation of the magnetization of the Mn at lower temperatures. The rectangular hysteresis of the 1-ML phase displayed in Fig. 2 shows again a simple in-plane magnetization loop.

The enhancement of the coercivity of the Co film by Sm can be qualitatively understood in terms of the Sm single-ion anisotropy<sup>13</sup>. The aspherical Sm 4f charge distribution is sensitive to the crystal field particularly at sites of reduced symmetry like at the surface. The temperature dependence of the magnetic behavior may be related to a mixing of the multiplet states  $J = 7/2$  and  $J = 9/2$  with the ground-state multiplet state  $J = 5/2$  of trivalent Sm due to the combined action of crystalline-electric and exchange fields<sup>14</sup>.

The presence of two magnetic elements, Sm and Co, raises the issue of their possibly different magnetic behaviour. In order to address this point, we performed element-specific magnetization measurements using reso-

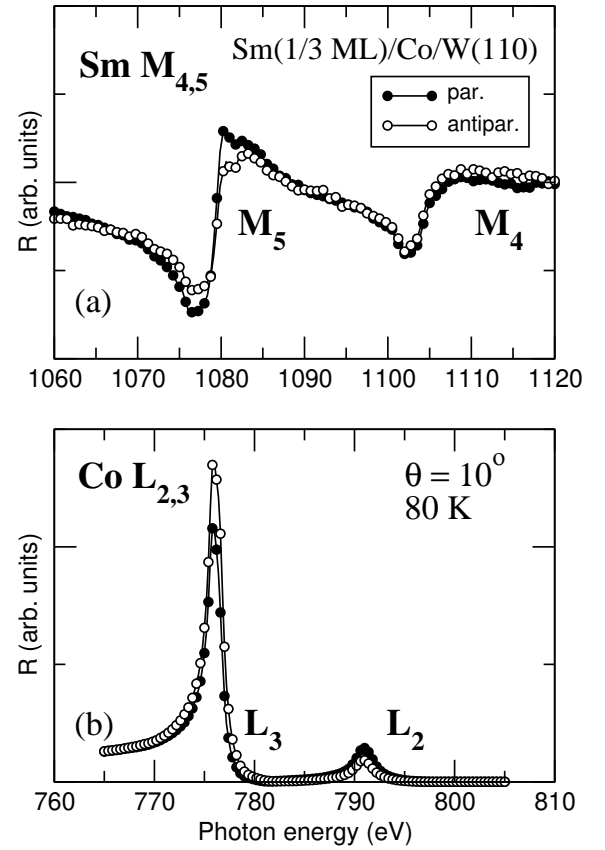


FIG. 4: Dichroic x-ray reflectivity spectra recorded across (a) the Sm  $M_{4,5}$  and (b) the Co  $L_{2,3}$  resonances of Sm(1/3 ML)/Co(10 ML)/W(110). Closed and open circles correspond to nearly parallel and antiparallel orientations of photon spin and sample magnetization, respectively.

nant soft x-ray scattering at elemental absorption thresholds. Figures 4 and 5 show soft x-ray reflectivity spectra measured on both of the studied Sm/Co(0001) ordered structures. The samples were permanently magnetized in-plane, and circularly polarized (CP) light was used with the photon spin almost parallel or antiparallel to the sample magnetization direction. Figure 4 corresponds to Sm(1/3 ML)/Co/W(110), Fig. 5 to Sm(1 ML)/Co/W(110). The spectra recorded across the Sm  $M_{4,5}$  and Co  $L_{2,3}$  thresholds are shown in the top (a) and bottom (b) panels of both figures, respectively.

The striking differences between the dichroic Co  $L_{2,3}$  reflectivity spectra displayed in Figs. 4b and 5b are mainly due to the different angles of x-ray incidence (10 and 20°, respectively), although the samples differ in Sm coverage and temperature as well. Similarly drastic changes in Co  $L_{2,3}$  specular reflectivity spectra with incidence angle have previously been observed.<sup>15</sup> They originate from interference, as the soft x-ray wavelength around the Co  $L_{2,3}$  edge is comparable to the Co film thicknesses in the nanometer scale. The photon-energy range extending to some 10 eV below the resonance max-

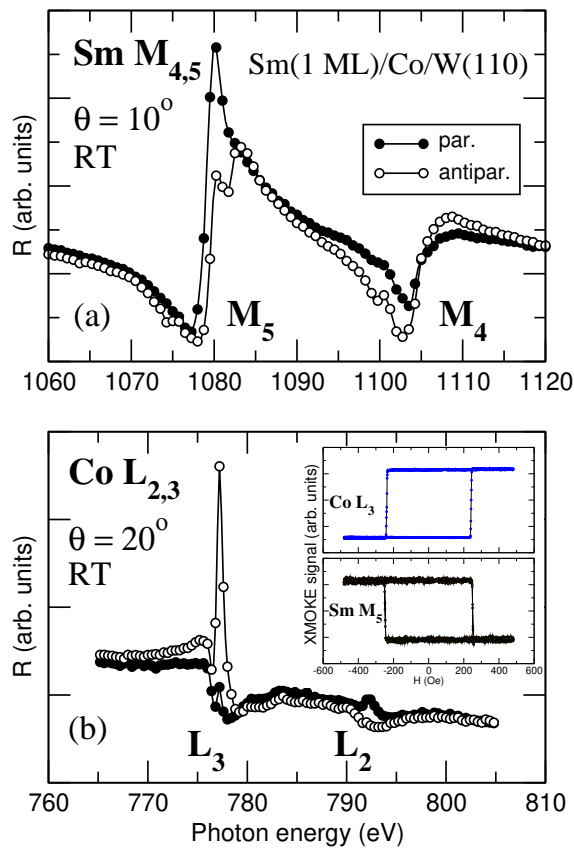


FIG. 5: Dichroic x-ray reflectivity spectra recorded across (a) the  $\text{Sm } M_{4,5}$  and (b) the  $\text{Co } L_{2,3}$  resonances of  $\text{Sm (1 ML)/Co (10 ML)/W (110)}$ . Closed and open circles correspond to nearly parallel and antiparallel orientations of photon spin and sample magnetization, respectively. The insert shows element-specific hysteresis loops measured at the  $\text{Sm } M_5$  and  $\text{Co } L_3$  maxima with an x-ray incidence angle of  $10^\circ$ .

in a is particularly sensitive to interference, favoured by the long x-ray penetration length due to reduced absorption (small imaginary part of the refractive index  $n$ ) and to the absence of total internal reflection (real part of  $n$  larger than 1).<sup>16,17</sup>

The spectra of both structures contain magnetic contrast, allowing to perform XMOKES measurements at the  $\text{Sm } M_5$  and  $\text{Co } L_3$  thresholds. XMOKES curves for the  $\text{Sm (1 ML)/Co/W (110)}$  phase recorded at an incidence angle of  $10^\circ$  are shown in the insert of Fig. 5(b). The reduced coercivity ( $H_c = 250 \text{ Oe}$ ) as compared to similar films displayed in Fig. 2a is mainly due to the different temperature; the slightly different Co thickness is known to play a minor role in this range.<sup>18</sup> The element-specific hysteresis loops of both elements reveal the same coercivity, showing that the film magnetization reverses simultaneously at the  $\text{Sm/Co}$  interface and deeper inside the Co film.  $\text{Sm/Co}$  films of different thicknesses showed always the same magnetic behaviour for the two elements.

Summarizing, we have found and characterized two ordered phases in the  $\text{Sm/Co}$  system. The  $\text{Sm (1 ML)/Co}$  phase shows an increased coercivity by a factor of 3 with respect to a pure Co film of the same thickness. Further experiments aiming at a detailed structural and morphological characterization of these phases are under way.

#### Acknowledgments

J.E. Prieto gratefully acknowledges financial support from the Alexander-von-Humboldt Stiftung and the Spanish MEC (EX2001). The authors thank F. Senf for experimental assistance at BESSY. This work was financed by the German BMBF (05KS1KEC/2).

Electronic address: josemilioprieto@uam.es; present address: Centro de Microanálisis de Materiales, Universidad Autónoma de Madrid, E-28049 Madrid, Spain

- <sup>1</sup> D. Mergel, H. Heilmann, and P. Hansen, *Phys. Rev. B* **47**, 882 (1993).
- <sup>2</sup> D. Weller and A. Moser, *IEEE Trans. Magn.* **35**, 4423 (1999).
- <sup>3</sup> J. F. Herbst, *Rev. Mod. Phys.* **63**, 819 (1991).
- <sup>4</sup> K. H. J. Buschow, *Rep. Prog. Phys.* **54**, 1123 (1991).
- <sup>5</sup> F. Heigl, O. K. Rupin, G. Kaindl, and K. Starke, *Rev. Sci. Instrum.* **73**, 369 (2002).
- <sup>6</sup> H. Fritzsch, J. Kohlhepp, and U. G. Radman, *Phys. Rev. B* **51**, 15933 (1995).
- <sup>7</sup> B. G. Johnson, P. Berlowitz, D. W. Goodman, and Bartholomew, *Surf. Sci.* **217**, 13 (1989).
- <sup>8</sup> J. G. Ociapa, P. J. Schultz, K. Grieths, and P. R. Norton, *Surf. Sci.* **225**, 281 (1990).
- <sup>9</sup> H. Knappe and E. Bauer, *Phys. Rev. B* **48**, 1794 (1993).
- <sup>10</sup> G. K. Wertheim and G. Cecelius, *Phys. Rev. Lett.* **40**,

- 813** (1978).
- <sup>11</sup> A. Stenborg, O. Björneholm, A. Nilsson, N. Martensson, J. Andersen, and C. Wignen, *Phys. Rev. B* **40**, 5916 (1989).
- <sup>12</sup> J. K. Lang and Y. Baer, *Solid State Commun.* **31**, 945 (1979).
- <sup>13</sup> D. Givord, J. Laforest, J. Schweizer, and F. Tasset, *J. Appl. Phys.* **50**, 2008 (1979).
- <sup>14</sup> K. H. J. Buschow, A. M. van Diepen, and H. W. de Wijn, *Solid State Commun.* **15**, 903 (1974).
- <sup>15</sup> C.-C. Kao, C. T. Chen, E. D. Johnson, J. B. Hastings, H. J. Lin, G. H. Ho, G. Meigs, J. M. Brot, S. L. Hulbert, Y. U. Idzerda, and C. Vettier, *Phys. Rev. B* **50**, 9599 (1994).
- <sup>16</sup> J. E. Prieto, F. Heigl, O. K. Rupin, G. Kaindl, and K. Starke, *Phys. Rev. B* **68**, 134453 (2003).
- <sup>17</sup> J. E. Prieto, O. K. Rupin, K. Dobrich, F. Heigl, G. Kaindl, and K. Starke, *Appl. Phys. A* **80**, 1021 (2005).
- <sup>18</sup> J. Camarero, J. J. de Miguel, A. Hernandez, and R. Miranda, *J. Appl. Phys.* **89**, 7150 (2001).